Journal of Alloys and Compounds 513 (2012) 510–517

Contents lists available at SciVerse ScienceDirect

Journal of Alloys and Compounds

journal homepage: www.elsevier.com/locate/jallcom

Small angle neutron scattering comparative investigation of Udimet 520 and Udimet 720 samples submitted to different ageing treatments

M. Rogante[a,*], V.T. Lebedev[b]

[a] Rogante Engineering Office, Contrada San Michele, n. 61, 62012 Civitanova Marche, Italy
[b] Petersburg Nuclear Physics Institute, Gatchina, St. Petersburg, Russia

ARTICLE INFO

Article history:
Received 5 September 2011
Received in revised form 22 October 2011
Accepted 29 October 2011
Available online 9 November 2011

Keywords:
Metals and alloys
Microstructure
Neutron scattering

ABSTRACT

Udimet 520 and Udimet 720 samples submitted to different annealing temperatures and ageing times have been investigated by small angle neutron scattering (SANS), with the aim to study precipitates phases microstructural evolution and materials' behaviour.

These materials are γ′ (Ni_3Al, Ti) precipitation hardened nickel-based superalloys possessing high strength, corrosion resistance and metallurgical stability. They are mainly adopted in high temperature environment, having found applications over a very wide range of temperature. Their importance has increased thanks to their good balance of mechanical properties and economic potential.

Information on the thermal treatment effects has been obtained, in particular concerning precipitate size and volume fraction distributions. The results contribute to confirm SANS to a level of industrial applicability in the considered sectors.

1. Introduction

New alloys and optimized procedures are progressively introducing innovative information for higher developments to replace conventional materials, with the main targets of enhancing efficiency and lengthening the duration of materials, components and facilities. Ni-based superalloys possess exceptional creep resistance and mechanical strength at high temperatures, in addition to corrosion and oxidation resistance; therefore, it is fundamental to improve their temperature capability, as well as to develop their manufacturing processes in order to widen the fields of their applications. These materials offer numerous possibilities to be used, mainly in high temperature environment, e.g., in turbo-machinery industry (for instance, jet engines, pump bodies and parts, gas turbines, power plants and rocket motors, subjected to steady and fluctuating stresses due, e.g., to centrifugal force and vibrations) and they have been identified as potential candidates for improved valve materials.

All these alloys have a matrix of γ with the major strengthening phase as γ′. High temperature fatigue strength has been identified as a critical factor in determining the performance of these materials. An evaluation of their microstructure, in correlation with partial information on the fatigue properties, shows that the volume fraction of the γ′ phase is likely to be a dominant factor in determining the characteristics at high temperatures. Since the size of the strengthening precipitates is also critical, it is anticipated that the kinetics of coarsening this phase would also be influential in the long-term performance of the alloys in this application [1].

The crucial parameters for the stability of Ni-based superalloys at high temperatures are yield stress, high elastic modulus and low thermal expansion coefficient [2,3], and excellent mechanical properties result also from their two-phase structure and grain boundaries strengthening by carbides. The duplex structure consists of γ′ precipitates (FCC ordered $L1_2$ structure) coherently embedded in the γ matrix (disordered FCC structure). In particular, the primary γ′ phase, consisting of aged coarse precipitates, is enclosed in a secondary finely dispersed phase, having a particle size ranging from few nm (secondary phase) to several hundreds of nm (primary phase). The γ′ phase is coherently formed within the FCC γ matrix after proper thermal treatment. The mechanical properties depend on the precipitates' size, spatial arrangement and volume fraction. The high temperature stability and deformation behaviour strongly depend on microstructural changes caused by complex operating thermo-mechanical conditions [2,4].

Udimet 520 (U520) is a low volume fraction γ′ precipitation hardenable Ni-based superalloy with an exceptional combination of high temperature mechanical properties, corrosion resistance and forgeability characteristics. The calculated major phase contents at 900 °C are (wt%): 77.6 (γ), 21.6 (γ′) and 0.8 (carbides) [1]. This alloy, developed for use in the 760–927 °C temperature range, possesses excellent structural stability and unusually good fabricability and it is recommended for applications where high strength at elevated temperatures is required. Primary uses are blading for aircraft and land-based gas

* Corresponding author. Tel.: +39 0733775248; fax: +39 07331941315.
E-mail address: main@roganteengineering.it (M. Rogante).

0925-8388/$ – see front matter © 2011 Elsevier B.V. All rights reserved.
doi:10.1016/j.jallcom.2011.10.106

turbines, as well as sheets and bolts for industrial and marine applications.

Udimet 720 (U720) is another Ni-based superalloy, solid solution strengthened with tungsten and molybdenum and precipitation hardened with titanium and aluminium. This material combines high strength with metallurgical stability, as demonstrated by excellent impact strength retention after long exposures at elevated temperatures. The calculated major phase contents at 900 °C are (wt%): 59.6 (γ), 40.0 (γ′) and 0.4 (carbides) [1]. Good oxidation and corrosion resistance combined with high strength make this alloy useful in gas turbine blade and disc applications. Moreover, Udimet 720, as well as Udimet 520, is being evaluated to be adopted in high temperature exhaust valves [1].

Various studies have been performed of both superalloys, in the last years, with the purpose of investigating their peculiarities and behaviours and increase their performances, also by developing thermodynamic modelling tools. Some of these models estimate different properties including those thermo-physical and physical, stress/strain graphs, stresses, hardness, coarsening of γ′ and γ″ and creep. The inclusion of micro-structurally sensitive parameters in these calculations, furthermore, allows connecting with materials' models to forecast micro-structure [5]. The investigation of the grain coarsening behaviour and $M_{23}C_6$ as well as secondary MC carbide precipitation kinetics in U520 showed that primary MC carbides and M(C, N) carbonitrides affect notably the grain growth, with their dissolution close to 1190 °C and 1250 °C, correspondingly, resulting in two different grain coarsening temperatures. The primary MC carbides are created during the solidification, while the secondary MC carbides may precipitate during an annealing or ageing process at temperatures less than the MC carbide solvus temperature [6]. Wrought U520 specimens were analyzed, to study the influence of different solutions and ageing processes on the dissolution and precipitation kinetics of γ′ and to assess the optimum pre- and post-forge heat treatment programmes. Double ageing treatments were performed at 925 °C/4 h/air cooled, followed by ageing at 700 or 800 °C for durations in the range 1–100 h. The precipitates' shapes resulted almost spherical at the beginning and, by enhancing the ageing time (especially at 800 °C), it appeared a partial change to cuboidal shapes [7]. U520 specimens were submitted to hot compression isothermal tests in the range 900–1150 °C with different strain rates, with the aim to analyze the deformation behaviour at high temperature. Tests at ≤950 °C led to fracture for all the adopted strain rates, while the flow behaviour at 1000, 1050 and 1075 °C indicated a dynamic recovery and, at higher temperatures, recrystallisation appeared as the softening mechanism [8]. Wrought U720 samples were submitted to tests in air at 700 °C under stress control, in order to investigate high temperature fatigue, creep and creep-fatigue properties. A creep dwell period was introduced in the fatigue loading conditions, resulting in a high enhance of the cyclic strain rate and in a decrease of the number of cycles to failure corresponding to the application of a short dwell time of 1 s. The higher the dwell time, the more detrimental resulted the outcomes on durability [9]. U720 specimens were submitted to hot compression tests in solution-treated conditions (simulating the forging process), to study their hot deformation behaviour. Samples were deformed in the temperature range 1000–1175 °C with different strain rates. A flow localization appeared for all the specimens under 1100 °C, as shear band through the diagonal direction and enhanced at upper strain rates. Tests in the range 1100–1150 °C resulted in a uniform deformation, with dynamic recrystallisation as the main flow softening mechanism over 1125 °C. Deformation exceeding γ′ solvus temperature was joined with grain boundary separation [10]. U720 samples were submitted to a solution treatment above the γ′ solvus temperature (to dissolve all γ′ before cooling at either a slow billet or a faster two-step intermediate cooling rate), in order to study, in comparison with other Ni-based superalloys, the response to ageing at 800 °C and the effects of composition and cooling rate on γ′ morphology, alloy hardness and γ–γ′ mismatch. The investigated materials, by cooling at a slow billet rate, followed the Lifshitz–Slyozov–Wagner theory (which predicts the coarsening rate for alloys), with an enhancement of the precipitate size by increasing the time and a formation of peak hardness in connection with a specific precipitate size [11]. Ni-based superalloys turbine blades for power plants, e.g., are generally working in very rigorous conditions, i.e. centrifugal loads, an extremely high temperature (800–1000 °C) of the gas, high temperatures gradient and vibrations. Such environment can involve a risk of material's failure associated with events like creep, high cycle fatigue, thermal fatigue and corrosion. Characterization of the precipitates is usually carried out by traditional methods such as image analysis, scanning electron microscopy (SEM), energy-filtered transmission electron microscopy (TEM), X-ray diffraction and theoretical modelling. First stage gas turbine blades for power plant (as received and after 31,325 engine operating hours at turbine inlet temperature of 1154 °C), made of wrought Udimet 520, were submitted to the following tests: optical and scanning electron microscopy to detect the microstructural constituents, hardness, force controlled fatigue, accelerated stress rupture adopting constant load creep testing machines and impact at 800 °C. The results showed, e.g., a dissolution of intra-granular MC carbide precipitates in the mid-section and a coarsening of continuous inter-granular precipitates in mid- and top section of the exercised blade, a degeneration at grain boundaries and a formation of σ phase in the mid and top section [12]. U720 samples cut from a land based gas turbine forged blade, solution treated at different temperatures for holding times in the range 2–24 h and successively quenched, were analyzed by using optical and scanning electron microscopy, to study the influence of diverse heat treatment conditions on the kinetics of γ′ precipitates dissolution, re-precipitation and growth. The obtained results included the evaluation of the γ′ solvus temperature (∼1150 °C), the assessment of the activation energy for γ′ coarsening (in the range 250–265 kJ/mol) and the estimate of a reference plot to predict the coarsening behaviour of γ′ in different heat treatment conditions [13].

SANS is a useful tool for materials characterization in the nanoscale range (1–100 nm), and although its full strength has not been employed yet, it presents the advantages of being non-destructive and providing information with high statistical exactness, due to the averaging over a macroscopic sample volume. Some earlier SANS studies of other Ni-based superalloy samples [14–16] and on real turbine buckets [17], for instance, have shown the measurement feasibility and the industrial applicability of the considered technique, which can supply complementary information to those obtained by TEM and SEM, where a very small area of the sample can be probed, thus resulting in a reduced statistical significance. The aim of our study is to recognize the structural features of these two types of alloys as dependent on the temperature (800–900 °C) and the ageing time (250–6000 h) in spatial scale $\sim 10^1$–10^2 nm responsible mainly for the functional properties of these materials.

2. Materials and methods

U520 and U720 10 mm × 10 mm × 2 mm samples submitted to different annealing temperatures and ageing times, as listed in Tables 1 and 2, have been investigated by using the V12 double crystal SANS diffractometer with bent crystals [18] at HMI, Berlin. This device (see the layout in Fig. 1) allows for the operation in the medium q-range and to overlap the q-gap between conventional SANS instruments and Bonse-Hart cameras. In our case, the adopted neutron wavelength was λ = 0.478 nm, while the instrumental device was adjusted to cover the range of momentum transfer from $q_{min} \sim 2 \times 10^{-3}$ nm^{-1} to $q_{max} \sim 8 \times 10^{-2}$ nm^{-1}. The nominal chemical composition of the considered materials is reported in Table 3.

Table 1
Udimet 520 samples and treatments.

Sample	Ageing time, h	Annealing temperature, °C
1	As-cast state	
2	1000	800
3	3000	800
4	6000	800
5	1000	900
6	3000	900
7	6000	900

Table 2
Udimet 720 samples and treatments.

Sample	Ageing time, h	Annealing temperature, °C
1	250	800
2	1000	800
3	3000	800
4	250	850
5	1000	850
6	3000	850
7	250	900
8	1000	900

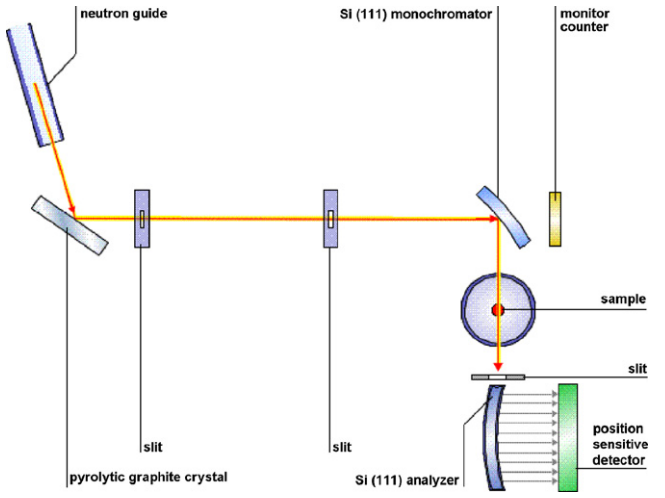

Fig. 1. Layout of the adopted SANS instrumentation.

SANS, among the different techniques allowing materials characterization in the nano-scale range 10^0–10^2 nm, has the advantage of being non-destructive and providing information with high statistical accuracy, due to the averaging over a macroscopic sample volume. The small absorption of neutrons, in particular, consents in many cases the investigation of centimetre thick material.

The data treatments are usually performed using the Guinier approximation. At all the annealing temperatures, the scattering intensity distributions can be described by the three-component Guinier model:

$$I(q) = \sum I_{i0} \cdot \exp\left[\frac{-(R_{Gi} \cdot q)^2}{3}\right] + B \quad (i = 1, 2, 3) \tag{1}$$

where

$$I_{i0} = K_i^2 \cdot N_i \cdot V_i^2 = K_i^2 \cdot \varphi_i \cdot V_i \tag{2}$$

is the intensity scattered from the particles fraction (being N_i the number of scatterers, R_{Gi} the gyration radius, V_i the volume, K_i the contrast and φ the volume fraction of particles), B is the incoherent background. For a detailed treatment of the theoretical bases, see Ref. [19–24].

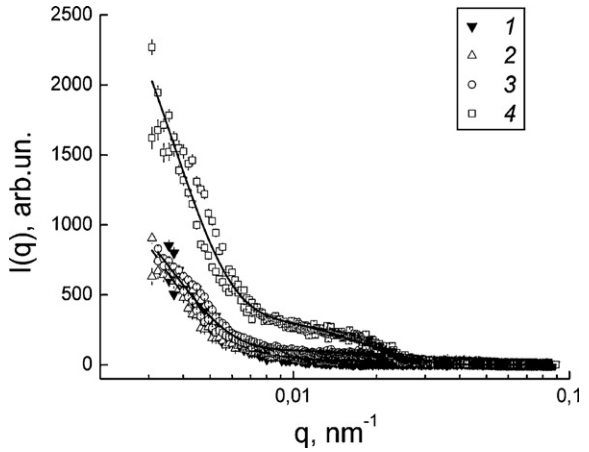

Fig. 2. SANS-intensities $I(q)$ vs. momentum transfer q for Udimet 520 as dependent on ageing time (800 °C): 1 – original sample, 2–4 – sample treated for 1000, 3000 and 6000 h respectively. Fitting curves correspond to the function (1).

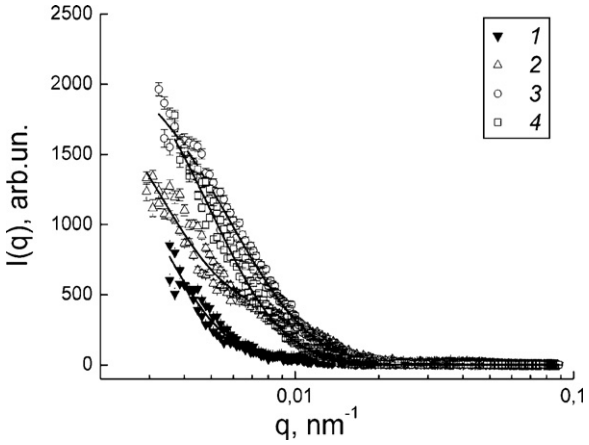

Fig. 3. SANS-intensities $I(q)$ vs. momentum transfer q for Udimet 520 as dependent on ageing time (900 °C): 1 – original sample, 2–4 – sample treated for 1000, 3000 and 6000 h respectively. Fitting curves correspond to the function (1).

3. Calculations, results and discussion

The SANS patterns for U520 superalloy, obtained respectively for the as-cast state and for the annealing at 800 and 900 °C, are displayed in Figs. 2 and 3 as dependent on the duration of the thermal treatment (t = 1000, 3000 and 6000 h). In these patterns, the final scattering data are displayed after the background subtraction and normalization on the instrumental curve. A substantial deviation of scattering curves (data 2–4) from that related to the original sample (data 1) was observed, as a result of ageing at 800 °C, only for long annealing time t = 6000 h (data 4) while at shorter times the effects of the thermal treatment on the nano-scale structure are weakly pronounced. It seems that at 800 °C a critical time 3000 h < t^* < 6000 h would exist, which should be exceeded to induce any visible structural changes. As a result of long-time heating, the SANS character in experimental q-range undergoes the evolution, with the appearance of at least two structural levels corresponding to the size of structural elements

Table 3
Nominal chemical composition of Udimet 520 and Udimet 720 superalloys (wt%).

Alloy	Ni	C	Al	Co	Cr	Mo	Nb	Ti	W	B	Zr
Udimet 520	Bal.	0.05	2.0	12.0	19.0	6.0	–	3.0	1.0	0.005	–
Udimet 720	Bal.	0.03	2.5	14.7	17.9	3.0	0.01	5.0	1.3	0.033	0.03

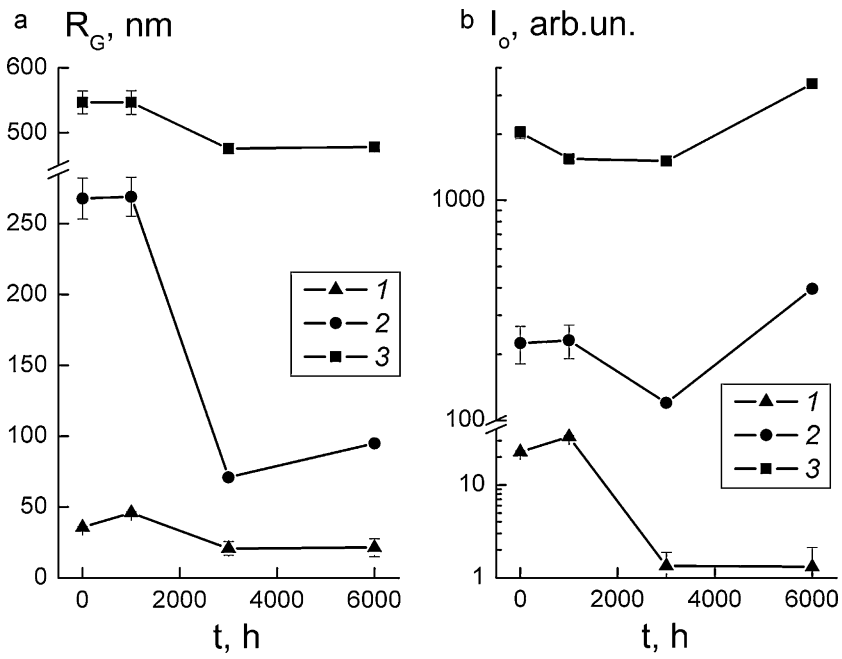

Fig. 4. Udimet 520 annealed at 800 °C. Data 1–3: gyration radii R_G (a) and forward scattering intensities I_0 (b) vs. ageing time t for the precipitates' fractions 1–3 (modes of scattering function (1), Table 4).

$R \sim 1/q \sim 100$ nm (hump on the scattering curve at $q \sim 0.01$ nm^{-1}, data 4) and $R > 100$ nm (strong growth of $I(q)$ at $q \leq 0.006$ nm^{-1}).

The temperature increase by 100 °C, on the other hand, makes the alloy's structure relatively labile. A possible critical time is reduced, $t^* < 1000$ h. This is evident from the patterns showing a progressive enhancement of intensity when the treatment time becomes longer, $t \sim 1000$–3000 h. A trend to saturation in structural evolution is observed, moreover, since the intensity at low $q \leq 0.01$ nm^{-1} for the maximum time $t = 6000$ h becomes slightly lesser with respect to that at $t = 3000$ h. The SANS-behaviour for annealing at 900 °C did not demonstrate such a discrete character of structuring as compared to Fig. 2 (data 4). Oppositely to the data at 800 °C, in Fig. 3 it is revealed a smooth monotonous increase of SANS-intensities in low-q-region for all ageing times.

Although some differences are found among the curves obtained for different ageing times, the final gains in scattering for both series of treatment are approximately at the same level. The growth of $I(q)$ by ~3 times at low $q \sim 0.003$ nm^{-1} (Figs. 2 and 3) indicates that, in general, a formation of large-scale structures (~10^2 nm) at 800 and 900 °C must be governed by the same mechanism, while the structuring rate depends on the temperature.

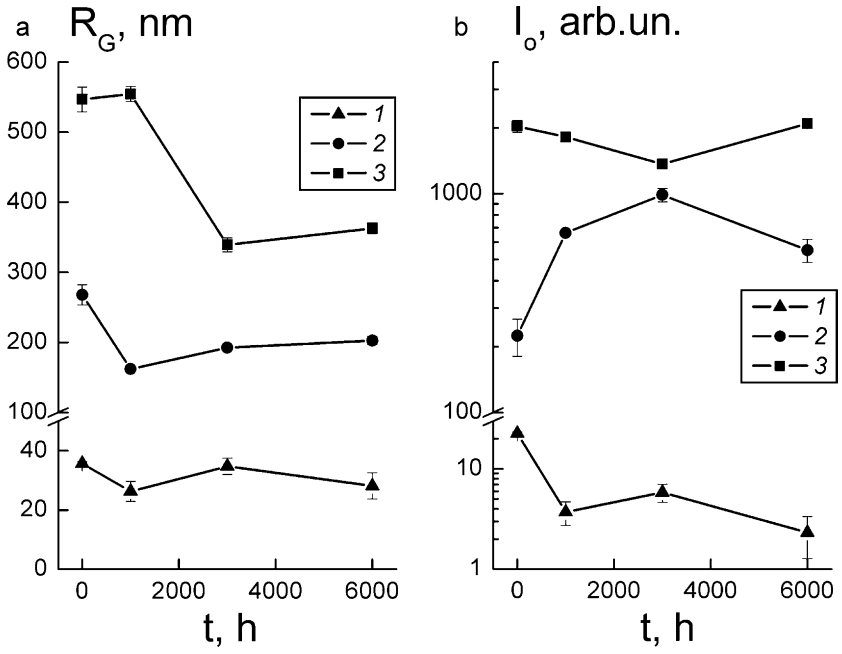

Fig. 5. Udimet 520 annealed at 900 °C. Data 1–3: gyration radii R_G (a) and forward scattering intensities I_0 (b) vs. ageing time t for the precipitates' fractions 1–3 (modes of scattering function (1), Table 4).

Table 4
Fitting parameters of scattering function (1) for Udimet 520 annealed at 800 and 900 °C.

T, °C	t, h	I_{01}, arb.un.	R_{G1}, nm	I_{02}, arb.un.	R_{G2}, nm	I_{03}, arb.un.	R_{G3}, nm
As received	–	22.7 ± 0.8	35.7 ± 0.6	224.0 ± 43.5	267.7 ± 14.4	2033 ± 130	546.7 ± 17.7
800	1000	33.1 ± 1.1	45.9 ± 0.8	231.0 ± 40.6	269.0 ± 13.7	1547 ± 82	546.6 ± 18.2
800	3000	1.3 ± 0.5	20.7 ± 4.8	120.0 ± 1.0	70.9 ± 0.6	1508 ± 26	475.8 ± 2.9
800	6000	1.3 ± 0.8	21.3 ± 6.3	396.4 ± 3.6	94.9 ± 0.7	3383 ± 66	478.4 ± 3.5
900	1000	3.7 ± 1.0	26.3 ± 3.4	662.6 ± 8.3	162.2 ± 1.1	1816 ± 89	554.3 ± 10.6
900	3000	5.8 ± 1.2	34.8 ± 2.8	987.3 ± 70.3	192.4 ± 3.4	1366 ± 55	339.2 ± 10.0
900	6000	2.3 ± 1.1	28.1 ± 4.4	552.2 ± 66.8	202.8 ± 6.0	2087 ± 49	362.8 ± 7.7

In order to understand the subtle features of structure evolution under thermal treatment, the data were approximated by the three-modal function (1), which describes all the data satisfactory at the fitting parameters given in Table 4.

The relationships between partial forward scattering intensities I_{ok} and gyration radii of corresponding fractions are clear visible in Figs. 4 and 5. The data from Table 4 are presented here to demonstrate the main features of structural transformation of U520 on spatial scales $R \sim R_G \sim 10^1$–10^2 nm. As it is seen from Fig. 3a, the long-time treatment (800 °C, $t > 1000$ h) caused the substantial decrease (factor ~2–3) of particles sizes belonging to small and middle fraction. The small fraction's scattering ability measured by the intensity I_{01}, moreover, dropped by an order of magnitude (Fig. 4b), so the contribution of small particles ($R_G \sim 20$ nm) to the scattering intensity becomes negligible. This can be a result of two processes. Firstly, one can suppose that the particles are destroyed into tiny fragments dissolved in the matrix. On the other hand, the particles of small fraction may aggregate. A remarkable growth of intensities I_{02} and I_{03} related to middle and large fraction, however, is observed only for the longest ageing time $t = 6000$ h, when small entities have disappeared by the heating during the time $t = 3000$ h.

The data in Fig. 4, therefore, testify the breaking of small structures and a relatively independent formation of middle- and large-size structures for a long time, $t \sim 6000$ h. It should be noted that such large-scale domains undergo only ~10% decrease in size even by long treatment ($t = 6000$ h), although the middle-sized entities show a disintegration (their gyration radius becomes lower by ~3 times, see Fig. 4a). At 800 °C, thus, the most stable structures are large-scale formations demonstrating a trend to progressive development by long-time annealing.

The structural peculiarities of alloy under the treatment at 900 °C were found still remarkably different (Fig. 5). Initially, it was assessed a decrease in size for large-scale domains (~30%). It is comparable to this effect (30–40%) for middle and small entities. All the structural elements, hence, do not result enough stable by the ageing. The scattering ability of small fraction has disappeared during the long-time annealing, while the big-size structures have shown practically the same forward scattering intensity. The middle-sized particles, however, have induced a huge growth in forward scattering intensity I_{02} (Fig. 5b): nevertheless, it is non-monotonous, showing a maximum at $t = 3000$ h. The discussed features of nanostructures can be understood more clearly by using a further data presentation. In Figs. 6 and 7, the parameters $I_0/R_{G3} \sim \phi$ proportional to volume content for each fraction $\varphi_{1,2,3}$ are presented as dependent on annealing time at 800 and 900 °C. It is assumed that the particles in all fractions possess the same contrast factor, $K_i = K$. The data in Fig. 6 exhibit a redistribution of different volume fractions in the alloy matrix. The ageing process at 800 °C during the time $t \geq 3000$ h leads to a decrease in the volume content φ_{01} of small-sized objects, while the volume parts of the 2nd and 3rd fractions demonstrate an enhancement. As a result, the 2nd type of particles dominates and the volume parts of other fractions still remain at a level being ~2 times lower than that related to the middle fraction. This redistribution, conversely, alters the sum volume part only slightly (data 4, Fig. 6) that guarantees the stable functional properties of the considered alloy.

At higher temperature (900 °C), on the other hand, the total content of inclusions does not remain constant (Fig. 7), dropping by a factor ~2 in the range of ageing time $t = 0$–6000 h. This is explained by the fact that the small fraction disappears but the content growth for the middle- and big-sized fractions is not enough to compensate the deficit. These data display a crucial influence of the temperature enhancement on nano-structure, defining alloy's stability regarding to mechanical properties.

The above used approach is based on the three-modal Guinier scattering function (1) to evaluate the structural parameters of U520 (gyration radii and the contribution of fractions to the total content of inclusions). The scattering data, except of inclusions' sizes, contain the information on the character of interface between these inclusions and the surrounding matrix. In the Porod's data presentation, this interface is revealed as a sharp border that is evident from the behaviour of modified intensity $q^4 I(q)$ (Fig. 8).

The function $q^4 I(q)$ achieves a saturation at $q \sim 0.02\ \text{nm}^{-1}$ that indicates the Porod's asymptotic behaviour $I(q) \sim 1/q^4$. Then, at higher $q > 0.025\ \text{nm}^{-1}$, the magnitudes of $q^4 I(q)$ decrease due to interference effects in scattering from the neighbouring particles.

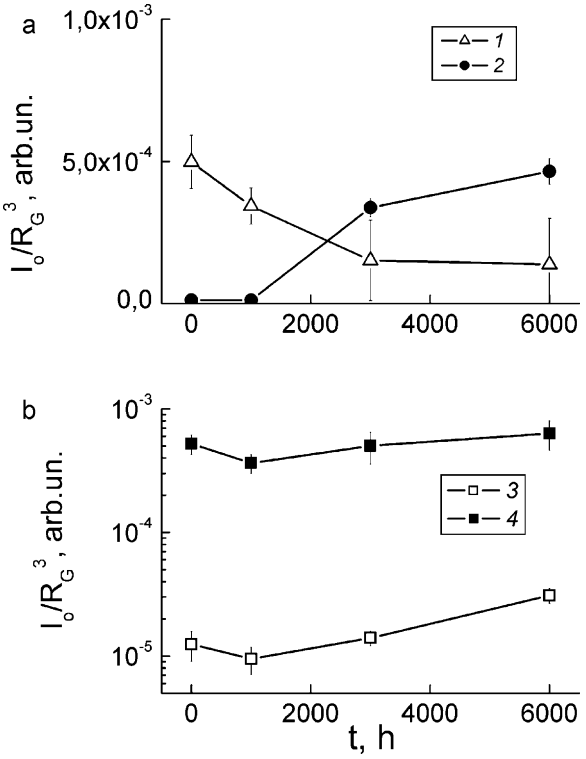

Fig. 6. Parameter $I_0/R_{G3} \sim \varphi$ being proportional to volume fractions for small, middle (1, 2) (a) and large (3) (b) structural elements in Udimet 520 vs. ageing time (800 °C). The sum of the parameters I_0/R_{G3} for all types of elements is shown in (b) (data 4).

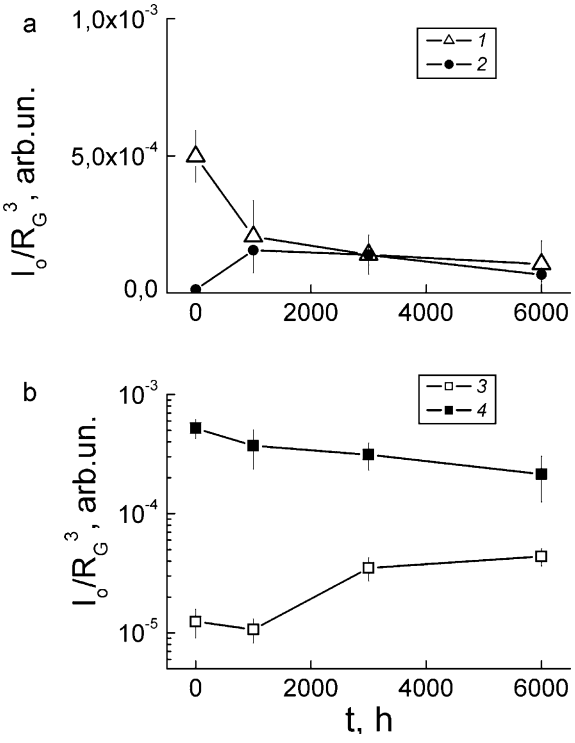

Fig. 7. Parameter $I_0/R_{G3} \sim \varphi$ being proportional to volume fractions for small, middle (1, 2) (a) and large (3) (b) structural elements in Udimet 520 vs. ageing time (900 °C). The sum of the parameters I_0/R_{G3} for all types of elements is shown in (b) (data 4).

The interference indicates a relatively high concentration of inclusions when the characteristic distances between them are comparable to their diameters. In the U520 alloy annealed at 800 °C for long time (t = 6000 h), the middle-sized particles dominate in the total volume of inclusions. The scattering data in the Porod's presentation, therefore, are described by the model function:

$$q^4 I(q) = Aq^4 F(q)^2 S(q) \quad (3)$$

for spherical particles (radius R_2, volume content φ_2) randomly distributed in matrix [25,26].

In (3), $A \sim K^2 \varphi_2 V_2$ is a parameter proportional to the contrast factor K for particles in matrix and $V_2 = (4\pi/3)R_2^3$ is the particle volume. Its form-factor:

$$F(q) = \left(\frac{3}{z^3}\right)[\sin(z) - z \cdot \cos(z)] \quad (4)$$

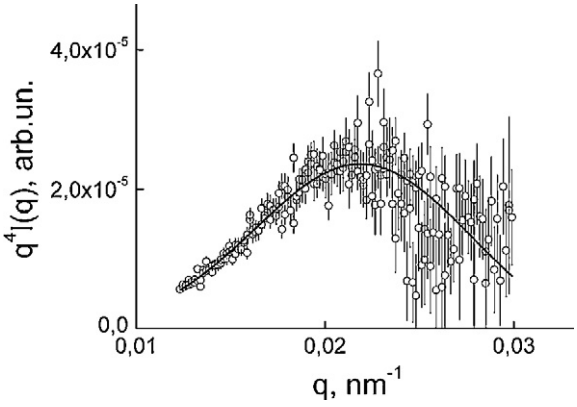

Fig. 8. SANS-data for Udimet 520 aged at 800 °C (t = 6000 h) in Porod's presentation, $q^4 I(q)$ vs. q. Curve is the approximation function (3).

Table 5
Partial (φ_{1-3}) and total (φ_t) volume fractions of inclusions in Udimet 520 treated at 800 and 900 °C for the times t = 0–6000 h.

T, °C	t, h	φ_1, vol.%	φ_2, vol.%	φ_3, vol.%	φ_t, vol.%
–	–	16.1 ± 4.0	0.4 ± 0.2	0.4 ± 0.1	16.9 ± 4.0
800	1000	11.1 ± 2.8	0.4 ± 0.2	0.3 ± 0.1	11.8 ± 2.8
800	3000	4.9 ± 4.0	10.9 ± 2.1	0.5 ± 0.1	16.3 ± 4.5
800	6000	4.4 ± 4.0	15.0 ± 1.5	1.0 ± 0.2	20.4 ± 4.4
900	1000	6.6 ± 4.4	5.0 ± 1.0	0.3 ± 0.1	11.9 ± 4.5
900	3000	4.5 ± 2.4	4.5 ± 1.4	1.1 ± 0.3	10.1 ± 2.8
900	6000	3.4 ± 2.8	2.1 ± 0.8	1.4 ± 0.3	6.9 ± 2.9

depends on the variable $z = qR_2$. The structural factor:

$$S(q) = \frac{1}{\{1 + 8\varphi_2(3/X^3)[\sin(X) - X \cdot \cos(X)]\}} \quad (5)$$

is a function of the variable $X = 2z$ and it is defined by the excluded volume, since the particles occupy a part (φ_2) of sample's volume. The function (3) approximates satisfactory the data (Fig. 7) at the following parameters: A = 544 ± 11 arb.un.; R_2 = 127.1 ± 1.0 nm; φ_2 = 15.0 ± 1.5 vol.%. It should be stated that the value of radius $R_2 \approx 127\,\text{nm} \approx (5/3)^{1/2} R_{G2} = 123 \pm 1.0\,\text{nm}$ is close to this one estimated from the gyration radius (Table 1) of uniform sphere. A comparison of the parameter $\phi_2 = I_{02}/R_{G2}^3$ and the total magnitude:

$$\Phi_t = \left[\frac{I_{o1}}{R_{G1}^3} + \frac{I_{o2}}{R_{G2}^3} + \frac{I_{o3}}{R_{G3}^3}\right] \quad (6)$$

in Fig. 6 (Table 1) provides the evaluation of total content of inclusions: $\varphi_{800\,^\circ\text{C}} = \varphi_2(\Phi_t/\Phi_2) = 20.4 \pm 4.4$ vol.% (t = 6000 h).

It should be noted that in this simplified consideration the model of spherical particles has been applied. The shape of inclusions, really, has to be close to the cubic one. Nevertheless, these cubes are obviously randomly oriented regarding to q-vector, i.e. a spherical symmetry in scattering exists. The comparison between the model scattering function for uniform sphere (radius R) and that for cubes (size A_{CUBE}) having the same gyration radius $R_G = A_{CUBE}/2 = (3/4)^{1/2}R$ [25,26] demonstrated very close behaviours: the deviation is small (≤1–5% in the range of $qR \le \pi$) and does not exceed the experimental errors shown in the presented data (e.g., in Fig. 7). Therefore, the application of the spherical approximation is correct. Finally, it is obtained the size of cubic particle $A_{CUBE2} = 2(3/5)^{1/2}R_2 = 197 \pm 2$ nm.

In similar way, from the data in Figs. 6 and 7 (Table 1) there was found the inclusions' volume fraction for U520 as received, i.e. $\varphi_0 = 16.9 \pm 4.0$ vol.% As a result of ageing at 900 °C (t = 6000 h), the volume part of inclusions was decreased by ~3 times, $\varphi_{900\,^\circ\text{C}} = \varphi_2(\Phi_t/\Phi_2) = 6.9 \pm 2.9$ vol.% For shorter ageing times (t = 1000, 3000 h) at 900 °C, the contents of inclusions were found ~12 vol.% and 10 vol.% respectively. These magnitudes are comparable, but they result ~2 times less than the values of $\varphi \sim 20\%$ reported in Ref. [1]. This discrepancy may be attributed to a possible presence of very large ($\ge 10^3$ nm) inclusions not detected in these SANS measurements. The partial and total fractions of inclusions in the U520 alloy, finally, are listed in Table 5.

The results for U520 differ remarkably from those related to U720. Similarly as above, the approximation of SANS-intensities was obtained for U720 by using the function (1). The SANS-patterns dependent on thermal treatment at 800, 850 and 900 °C are shown in Figs. 9–11 and the fitting parameters are summarized in Table 6. As compared to U520, in the U720 samples three types of structural element were found only at 800 °C for the ageing times t = 250 and 1000 h. During a longer treatment (t = 3000 h), the small and large structures result destroyed, while only the middle-size inclusions demonstrate stability in size and scattering ability (Table 6).

At higher temperatures (850 and 900 °C, Table 6) the middle-sized particles prevail, while only a low amount of small particles was found after the treatment for short time t = 250 h (900 °C).

Table 6
Fitting parameters of scattering function (1) for Udimet 720 annealed at 800, 850 and 900 °C.

T, °C	t, h	I_{01}, arb.un.	R_{G1}, nm	I_{02}, arb.un.	R_{G2}, nm	I_{03}, arb.un.	R_{G3}, nm
800	250	352.3 ± 31.7	120.6 ± 2.6	1308 ± 53	225.2 ± 5.9	3074 ± 58	447.6 ± 7.9
800	1000	42.5 ± 19.0	93.7 ± 6.5	901 ± 16	159.0 ± 2.8	3253 ± 29	374.9 ± 2.9
800	3000	–	–	931 ± 5	187.2 ± 0.6	–	–
850	250	–	–	625 ± 5	178.3 ± 0.8	–	–
850	1000	–	–	547 ± 7	200.3 ± 1.4	–	–
850	3000	–	–	639 ± 35	160.3 ± 2.3	1249 ± 28	302.5 ± 6.3
900	250	11.5 ± 3.6	81.6 ± 8.4	965 ± 7	225.0 ± 1.5	–	–
900	1000	–	–	1536 ± 26	190.4 ± 1.0	1987 ± 59	436.3 ± 8.6

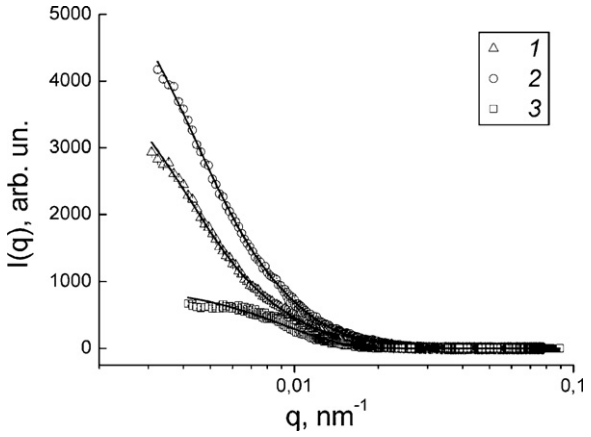

Fig. 9. SANS-intensities $I(q)$ vs. momentum transfer q for Udimet 720 as dependent on ageing time (800 °C): 1–3–sample treated for 250, 1000 and 3000 h respectively. Fitting curves correspond to the function (1).

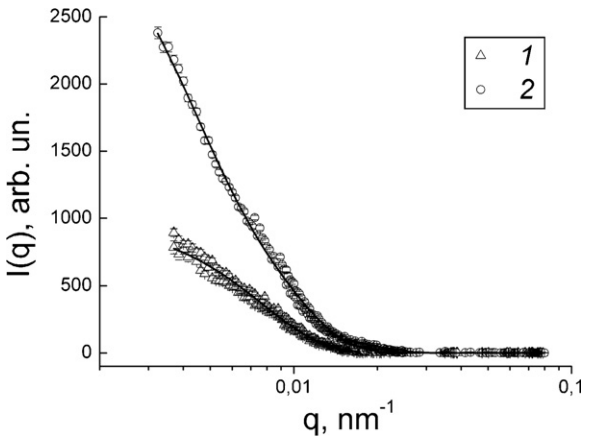

Fig. 11. SANS-intensities $I(q)$ vs. momentum transfer q for Udimet 720 as dependent on ageing time (900 °C): 1, 2–sample treated for 250 and 1000 h. Fitting curves correspond to the function (1).

A longer heating (t = 1000, 3000 h) did not initiate any formation of small particles, but caused the structuring at middle and large spatial levels ($R_{G2} \sim 200$ nm, $R_{G3} \sim 300$–400 nm, see Table 6). The U720 material trends to generate the inclusions with gyration radii ~200–400 nm, being in average better than the precipitates in U520 (gyration radii ~20–500 nm).

The volume fractions of inclusions in U720 have been finally assessed. With this purpose, the data for the ageing at 850 °C (t = 1000 h) were plotted in the Porod's presentation, showing an increase of the modified intensity $q^4I(q)$ up to saturation at $q \sim 0.01$ (Fig. 12). At higher q-magnitudes the modified intensity comes down due to some interference effects in scattering from the neighbouring particles. It is important that in U720 aged at 850 °C for 250 and 1000 h there were found only middle-sized particles (Table 3). It was applied, hence, the approximation with the model function (3) for uniform spherical particles (radius R_2) randomly distributed in the sample's volume. The fitting with function (3) gives the following parameters: $A = 670 \pm 14$ arb.un.; $R_2 = 257.6 \pm 1.0$ nm; $\varphi_2 = 9.2 \pm 0.9$ vol.% (850 °C, t = 1000 h).

As above reported, the radius R_2 of the effective spherical particle gives the size $A_{CUBE2} = 2(3/5)^{1/2}R_2 = 399 \pm 2$ nm of the corresponding cubic inclusions.

The value of $\varphi_0 = 9.2 \pm 0.9$%vol. (treatment at 850 °C, t = 1000 h), then, has served as a reference parameter to compute the partial and total volume fractions for the data at 850 and 900 °C (Table 7). It was obtained in a similar way as above, i.e. by using the magnitudes of forward scattering intensities and gyration radii (Table 6).

As compared to U520, the U720 alloy possesses a higher ability to form precipitates whose total concentration surpasses that related to U520 by a factor 2–3 (Table 7). At the temperature 800 °C (t = 1000 h), e.g., in U720 the total content of

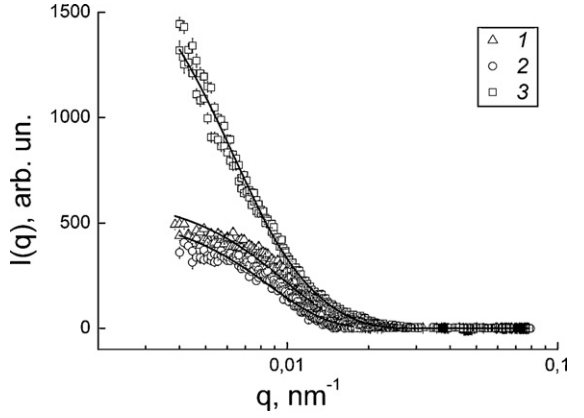

Fig. 10. SANS-intensities $I(q)$ vs. momentum transfer q for Udimet 720 as dependent on ageing time (850 °C): 1–3–sample treated for 250, 1000 and 3000 h. Fitting curves correspond to the function (1).

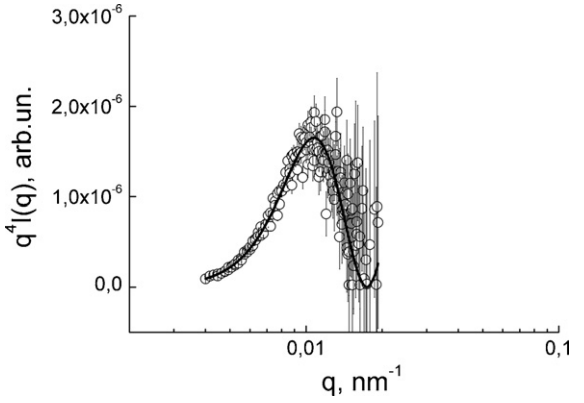

Fig. 12. SANS-data for Udimet 720 aged at 850 °C (t = 1000 h) in Porod's presentation, $q^4I(q)$ vs. q. Curve is the approximation function (3).

Table 7
Partial (φ_{1-3}) and total (φ_t) volume fractions of inclusions in alloy Udimet 720 treated at 800, 850 and 900 °C during the times t = 250–3000 h.

T, °C	t, h	φ_1, vol.%	φ_2, vol.%	φ_3, vol.%	φ_t, vol.%
800	250	27.2 ± 4.1	15.5 ± 2.1	4.6 ± 0.5	47.5 ± 6.5
800	1000	7.0 ± 3.5	30.3 ± 3.5	8.3 ± 0.9	45.6 ± 9.7
800	3000	–	19.2 ± 2.0	–	19.2 ± 2.0
850	250	–	14.9 ± 1.5	–	14.9 ± 1.5
850	1000	–	9.2 ± 0.9	–	9.2 ± 0.9
850	3000	–	21.0 ± 2.6	6.1 ± 0.7	27.1 ± 2.7
900	250	2.9 ± 1.3	11.4 ± 1.2	–	14.3 ± 1.8
900	1000	–	30.1 ± 3.2	3.2 ± 0.4	33.3 ± 3.2

inclusions resulted $\varphi_t \sim 46$ vol.%, while the U520 sample contained only $\varphi_t \sim 12$ vol.% of precipitates. Roughly is kept also at higher temperature (900 °C, t = 1000 h): in U720, it results $\varphi_t \sim 33$ vol.%, while in U520 it results $\varphi_t \sim 12$ vol.%

The obtained concentrations lay at the level of estimates given for the U520 and 720 (~20 and 40%) [1]. This should be considered as a really satisfactory agreement, since our data and the estimates of Ref. [1] relate to different samples.

4. Conclusions

SANS has enables us studying the structural evolution after thermal treatments of U520 and U720 superalloys at a nano-scale level and evaluating the precipitates' dimensions and volume contents. Although these alloys have a relatively close each other chemical composition, they exhibit a very different ability to form precipitates at the temperatures 800–900 °C.

U520 demonstrated a growth of inclusions in a wide range of sizes (~20–500 nm), while their volume content does not exceeded 20%. U720, on the other hand, exhibited a stronger tendency in structuring, which was revealed by the formation of larger domains in the matrix (gyration radii ~200–400 nm, content ~10–40%), while small-sized structures were practically not observed. The U720 alloy, as compared to U520 under the same conditions, may form a more regular nano-structure, which promotes in its stability and strengthening.

The adopted technique is suitable to be regularly exploited for the accumulated damage evaluation in the considered materials and components.

Acknowledgement

EC support for access to the BENSC facilities is acknowledged.

References

[1] FY 2006 Progress Report for Automotive Propulsion Materials Program, U.S. Department of Energy Office of Freedom CAR and Vehicle Technologies, Washington, 2007.
[2] T. Khan, P. Caron, in: E. Bachelet, et al. (Eds.), High Temperature Materials for Power Engineering. Part II, Kluwer Academic Publishers, Dordrecht, The Netherlands, 1990, pp. 1261–1270.
[3] R.V. Curtis, R.N. Ghosh, M. Mc Lean, Creep and Fracture of Engineering Materials and Structures, The Institute of Materials, London, 1993.
[4] J. Zrník, Influence of thermal and stress loading on the structure of nickel superalloys, Habilitation Thesis, Department of Material Sciences, Technical University of Košice, Slovakia, 1990.
[5] N. Saunders, Z. Guo, X. Li, A.P. Miodownik, J-Ph. Schillé, in: K.A. Green, T.M. Pollock, H. Harada, T.E. Howson, R.C. Reed, J.J. Schirra, S. Walston (Eds.), Proc. Int. Conf. Superalloys 2004, The Minerals, Metals & Materials Society, Warrendale, USA, 2004, pp. 849–858.
[6] S. Xu, J.I. Dickson, A.K. Koul, Metall. Mater. Trans. A 29A (1998) 2687–2695.
[7] M. Jahazi, A.R. Mashreghi, Mater. Sci. Technol. 18 (2002) 458–462.
[8] A.R. Mashreghi, H. Monajatizadeh, M. Jahazi, S. Yue, Mater. Sci. Technol. 20 (2004) 161–166.
[9] T. Billot, P. Villechaise, M. Jouiad, J. Mendez, Int. J. Fatigue 32 (2010) 824–829.
[10] H. Monajati, M. Jahazi, S. Yue, A.K. Taheri, Metall. Mater. Trans. A 36 (2005) 895–905.
[11] R.J. Mitchell, M. Preuss, Metall. Mater. Trans. A 38 (2007) 615–627.
[12] A.K. Ray, S.R. Singh, J. Swaminathan, P.K. Roy, Y.N. Tiwari, S.C. Bose, R.N. Ghosh, Mater. Sci. Eng. A 419 (2006) 225–232.
[13] H. Monajati, M. Jahazi, R. Bahrami, S. Yue, Mater. Sci. Eng. A 373 (2004) 286–293.
[14] M. Rogante, V.T. Lebedev, Mater. Des. 29 (2008) 1060–1065.
[15] M. Rogante, V.T. Lebedev, in: L. Petterson, G.M. Cojazzi (Eds.), Proc. 31st ESReDA Seminar, EUR 22887 EN, European Communities, Ispra, Italy, 2006, pp. 58–68.
[16] V.T. Lebedev, M. Rogante, in: K. Grilec (Ed.), Proc. Int. Conf. "MATRIB'05", Croatian Society for Materials and Tribology, Zagreb, Croatia, 2005, pp. 133–138.
[17] M. Rogante, J. Šaroun, P. Strunz, G.F. Ceschini, V. Ryukhtin, P. Lukáš, V. Marinčák, Kovove Mater. 43 (2005) 371–381.
[18] T. Robertson, H.A. Graf, R. Michaelsen, P. Vorderwisch (Eds.), Neutron-Scattering Instrumentation at the Research Reactor BER II, Hahn-Meitner-Institut, Berlin, 1996.
[19] G. Kostorz, in: G. Kostorz (Ed.), Treatise on Materials Science and Technology, Academic Press, New York, 1979, pp. 227–289.
[20] O. Glatter, O. Kratky, Small Angle X-ray Scattering, Academic Press, New York, 1982.
[21] C. Williams, R.P. May, A. Guinier, Mater. Sci. Technol. 2B (1994) 611–656.
[22] H.M. Rietveld, Acta Crystallogr. 22 (1967) 151–152.
[23] H.M. Rietveld, J. Appl. Crystallogr. 2 (1969) 65–71.
[24] M. Rogante, in: M. Rogante (Ed.), Proc. on the 1st Italian Workshop for Industry "Applicazioni Industriali delle Tecniche Neutroniche®", Rogante Engineering, Civitanova Marche, Italy, 2008, pp. 40–120.
[25] A. Guinier, G. Fournet, Small-Angle Scattering of X-rays, J. Wiley & Sons, Inc., London, 1955.
[26] D.I. Svergun, L.A. Feigin, X-ray and neutron small-angle scattering, Nauka, Moscow, 1986.

Further reading

[27] R.C. Reed, M.P. Jackson, Y.S. Na, Metall. Mater. Trans. A 30 (1999) 521–533.
[28] M.J. Johnson, B. Zhu, C.C.H. Lo, D.C. Jiles, R.E. Shannon, AIP Conf. Proc. 557/1 (2001) 1429–1436.
[29] S. Xu, A.K. Koul, J.I. Dickson, Metall. Mater. Trans. A 32 (2001) 795–804.
[30] R.C. Reed, The Superalloys: Fundamentals and Applications, Cambridge University Press, New York, 2006.